

# Exploring the phase space of the quantum delta kicked accelerator

G. Behinaein, V. Ramareddy, P. Ahmadi, and G.S. Summy

*Department of Physics, Oklahoma State University, Stillwater, Oklahoma 74078-3072*

We experimentally explore the underlying pseudo-classical phase space structure of the quantum delta kicked accelerator. This was achieved by exposing a Bose-Einstein condensate to the spatially corrugated potential created by pulses of an off-resonant standing light wave. For the first time quantum accelerator modes were realized in such a system. By utilizing the narrow momentum distribution of the condensate we were able to observe the discrete momentum state structure of a quantum accelerator mode and also to directly measure the size of the structures in the phase space.

PACS numbers: 05.45.Mt, 03.75.Kk, 32.80.Lg, 42.50.Vk

For more than a century the study of chaotic phenomena has been recognized as being crucial to developing a fuller understanding of nature. One aspect of this study which was missing until relatively recently was experimental scrutiny of quantum systems which in the classical limit exhibit chaotic behavior. Theoretical work on this subject had largely concentrated on the investigation of idealized systems such as the quantum delta-kicked rotor (QDKR) which were already well known from extensive work in the classical regime [1]. The experimental study of this system gained new impetus through its realization using laser cooled atoms exposed to a corrugated potential from a pulsed off-resonant standing light wave [2]. This system has subsequently led to many discoveries in the field of quantum chaos including observation of quantum resonances [2, 3], dynamical localization [4, 5] and quantum diffusion [6, 7]. In the theoretical description of the QDKR the effective value of Planck's constant scales with the time between the pulses [8, 9]. Therefore, to achieve classical correspondence in which  $\hbar \rightarrow 0$ , the time between pulses needs to be close to zero. However, for technical reasons this value can not be made arbitrarily small in experiments.

Recently, Fishman, Guarneri, and Rebbuzzini (FGR) [10] have shown that this difficulty can be circumvented for kicking periods close to a quantum resonance time. These resonance times [11, 12] occur at integer multiples of the Talbot time, a time interval during which plane waves with certain equally spaced momenta in the kicking direction can acquire a phase factor which is an integer multiple of  $2\pi$ . This is analogous to the Talbot effect in optics [13]. Using this method, FGR have studied the quantum delta-kicked accelerator (QDKA) which can be created by taking the QDKR and adding a linear potential along the direction of the standing wave. They showed that the effective value of Planck's constant scales with the deviation of the pulse separation time from certain non-zero resonance times, thus making it feasible to make the effective Planck's constant very small. Therefore, if the time between pulses is chosen close to these resonance times, a pseudo-classical approach can be adopted to study the system.

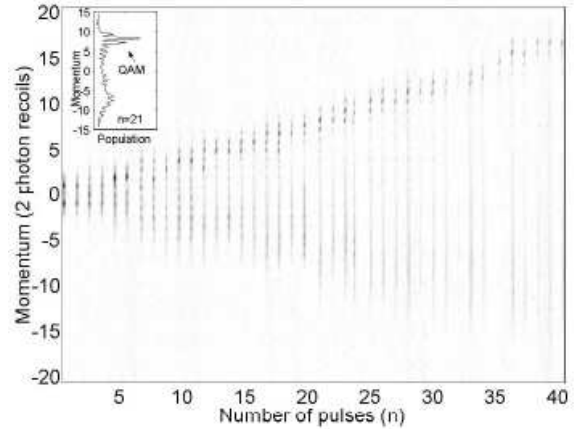


FIG. 1: Experimental momentum distributions showing a QAM in a BEC exposed to a series of kicks from a standing light wave in the free falling frame. The kicking period was  $72.2 \mu\text{s}$  and the momentum distributions are displaced as a function of the number of kicks. The accelerator mode is the collection of momentum states that appear to move towards the upper right. The inset shows the momentum distribution for a pulse number of  $n=21$ .

Perhaps the simplest way of experimentally realizing the QDKA is by applying the pulsed standing wave in the direction of gravity [14, 15]. This experiment has led to the discovery of quantum accelerator modes (QAMs) near the resonance times. One of the most important characteristics of QAMs is that they are comprised of atoms which show a linear momentum growth with pulse number in a freely falling frame [15]. It has been shown that QAMs are quantum nondissipative counterparts of mode locking [16]. They have also been suggested for use in the preparation of well defined initial conditions for quantum chaos experiments [17]. FGR attributed the QAMs to the existence of stability islands in the pseudo-classical phase space. These studies have shown that this underlying phase space has a complex structure which is highly sensitive to the experimental parameters. However, the broad momentum distribution of the laser cooled atoms which have been used so far to study this

system have prevented the examination of the local structures in the phase space.

In this letter we report on the realization of QAMs using a Bose-Einstein condensate (BEC) of rubidium 87 atoms and the exploration of the pseudo-classical phase space structure of the QDKA. Figure 1 shows experimentally observed momentum distributions as a function of the number of standing wave pulses applied to a BEC. This figure demonstrates that the QAM gains momentum linearly as the number of pulses increases. Note that this is the first time that it has been possible to determine that the QAM is made up of several distinct momentum states as originally postulated in Ref. [14]. This quantization of momentum is observable because the initial momentum uncertainty of the condensate was much smaller than two photon recoils.

The Hamiltonian of the delta kicked accelerator for an atom with mass  $m$  can be written as,  $H = p^2/2m + mg'x + \frac{U_{\max}}{2}[1 + \cos(Gx)]\sum_n \delta(t - nT)$ , where  $p$  is the atomic momentum along the standing wave,  $g'$  is the component of the gravitational acceleration in the direction of the standing wave,  $G = 2k$  the grating vector where  $k$  is the light wave vector,  $n$  the pulse number,  $T$  the pulse period, and  $U_{\max}$  is the well depth of the standing wave due to the light shift. The net effect of the time dependent potential is to distribute the condensate into different momentum states via a diffractive process. The population of these momentum states is determined by  $|J_{n'}(\phi_d)|^2$ , where  $J_{n'}(\phi_d)$  is an  $n'$ th order Bessel function of the first kind with argument  $\phi_d = U_{\max}\Delta t/(2\hbar)$ , the phase modulation depth [14]. It is useful to consider this system for pulse periods close to integer multiples of the half Talbot time,  $T_\ell = \ell \times 2\pi m/\hbar G^2 (= \ell \times 33.3\mu\text{s}$  for Rb87 atoms). With this restriction the system can be described by the classical map [10],

$$\begin{aligned} \theta_{n+1} &= \theta_n + \text{sgn}(\epsilon)J_n \\ J_{n+1} &= J_n - K \sin(\theta_{n+1}) + \text{sgn}(\epsilon)\tau\eta, \end{aligned} \quad (1)$$

where  $\epsilon = 2\pi\ell(T/T_\ell - 1)$  is a small number,  $\ell$  is any positive integer number, and  $K = |\epsilon|\phi_d$ . The dimensionless  $J$  and  $\theta$  parameters are defined as,

$$\begin{aligned} \theta &= Gx \bmod(2\pi) \\ J_n &= I_n + \text{sgn}(\epsilon)[\pi\ell + \tau(\beta + n\eta + \eta/2)] \end{aligned} \quad (2)$$

where  $p/(\hbar G) = I/|\epsilon| + \beta$ ,  $\beta$  is the fractional momentum,  $\tau = \hbar T G^2/m$ , and  $\eta = mg'T/(\hbar G)$ . Figure 2 shows a typical phase space portrait for the map of Eq. (1) with  $\phi_d = 1.4$ ,  $T = 29.5\mu\text{s}$  and  $\epsilon = -0.72$ . Perhaps the most important feature of this plot is the existence of a stable fixed point surrounded by an island of stability. If the size of these islands is large enough to capture a significant fraction of the wavepacket they give rise to observable accelerator modes. According to this model the momentum gain of an atom in a period  $\mathbf{p}$  accelerator mode after

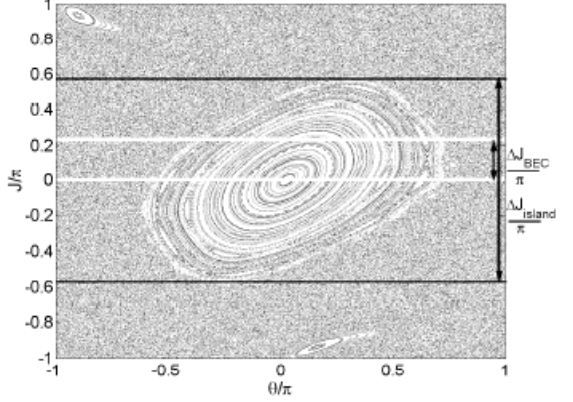


FIG. 2: Phase space unit cell for the QDKA map of Eq. (1) with  $\phi_d = 1.4$  and  $T = 29.5 \mu\text{s}$ . A stable fixed point with  $(\mathbf{p}, \mathbf{m}) = (1, 0)$  exists at  $J = 0$  and  $\theta = 0.0887$ . This stable fixed point is surrounded by the stability island in which the quantum accelerator mode will be created if the atomic initial conditions are inside the island. The momentum width of the condensate,  $\Delta J_{\text{BEC}}$  and the stability island  $\Delta J_{\text{island}}$ , are shown with the solid white and black lines respectively.

$n$  kicks is given by,

$$q = n \left[ \frac{\eta\tau}{\epsilon} + \frac{2\pi\mathbf{m}}{\mathbf{p}|\epsilon|} \right], \quad (3)$$

where  $\mathbf{m}$  is an integer and  $(\mathbf{p}, \mathbf{m})$  specifies a particular accelerator mode [10, 16, 18].

The initial conditions of atoms that can be accelerated is another important property of the accelerator modes. The limited range of these conditions is a consequence of the fact that the stability islands do not cover the whole unit cell of the phase space. Furthermore, the initial momentum required for an accelerator mode to emerge is periodic. This can be seen by using Eq. (2) and the fact that  $J$  has a periodicity of  $2\pi$ . This is equivalent to a momentum periodicity of  $\Delta p = 2\pi\hbar G/\tau$ . Observing this phase space structure requires that the atomic momentum distribution be narrower than  $2\pi\hbar G/\tau$ . This implies a temperature of  $\approx 450$  nK for Rb87 atoms exposed to a pulsed standing wave of 390 nm wavelength and pulse period close to the Talbot time ( $\ell = 2$ ). To this extent, a BEC is an ideal candidate [19]. The momentum width of a condensate is shown with two white lines in Fig. 2. Note that this width is smaller than the momentum extent of the island, indicating that the momentum resolution of the experiment is more than sufficient to clearly detect and identify a stability island from the chaotic background. However, for experiments utilizing cold thermal atomic samples, the momentum distribution is significantly wider than  $\hbar G$ . Although this wide momentum distribution makes it relatively easy to observe the accelerator modes, there is no direct way of

examining the structure of the phase space.

In order to use BEC to explore the phase space of the kicked accelerator we used the experimental setup described in detail by Ref.[20]. A standard six-beam MOT was used to trap about  $50 \times 10^6$  atoms which were loaded into the trapping potential created by a focused CO<sub>2</sub> laser beam. In order to optimize the loading efficiency, the waist of the beam was chosen to be 100  $\mu\text{m}$  [21]. Typically  $4 \times 10^6$  atoms were trapped at the focus of the CO<sub>2</sub> laser beam. Subsequently, one of the lenses through which the beam passed was moved 17 mm in 1 s so as to reduce the beam waist to 12  $\mu\text{m}$  and compress the trap for efficient evaporative cooling [22]. The power in the beam was then reduced to 100 mW in 4 s to create a pure condensate with  $\sim 50000$  atoms in the  $5S_{1/2}F = 1, m_F = 0$  state. The CO<sub>2</sub> laser was then turned off and after a variable time interval the kicking potential was turned on. Varying this time allowed the BEC to fall under the influence of gravity, thus changing the momentum of the condensate at the commencement of the kicks. The light for the kicks was obtained by passing the light from the MOT laser through a 40 MHz acousto-optic modulator (AOM). This light was 6.7 GHz red detuned from the  $5S_{1/2}F = 1 \rightarrow 5P_{3/2}F = 2$  transition of Rb87 and propagated at 41° relative to the vertical direction. The beam size was 1 mm, such that  $\phi_d$  did not change appreciably while the BEC was interacting with the series of kicks. The phase modulation depth,  $\phi_d$ , was inferred by comparing the population of the first and zeroth order momentum states after one pulse. The temporal profile of the standing light wave was controlled by periodically switching the AOM on in order to create a sequence of pulses each 250ns in length. The momentum distribution was measured using a time of flight method. That is, the condensate expanded for a controlled time interval, typically 9 ms, and was then destructively imaged using an absorptive technique.

To observe the pseudo-classical phase space structure of the QAMs, a series of data were taken for pulse periods near both Talbot and half-Talbot times. Figure 3 shows a typical data set taken at (a)  $T = 61\mu\text{s}$ , (b)  $T = 72.2\mu\text{s}$ , (c)  $T = 28.5\mu\text{s}$ , and (d)  $T = 37.1\mu\text{s}$  pulse separations for different values of the BEC's initial momentum. (a) and (b) occur on either side of the Talbot time at  $T = 66.6\mu\text{s}$  while (c) and (d) occur on either side of the half-Talbot time at  $T = 33.3\mu\text{s}$ . The data in Figure 3 was created by horizontally stacking 60 time-of-flight images of the condensate, each for a different initial momentum. These data confirm the periodicity of the QAMs with momentum. Furthermore, the data of Fig. 3 provides a direct way to validate the theoretical prediction of the island size. To do so, the data of Fig. 3 was summed along the initial momentum axis.  $\Delta p_{\text{island}}$  was then determined by measuring when the accumulated signal of the QAM had dropped to  $1/e$  of its maximum value. The theoretical values were inferred by plotting the map of Eq.(1) for

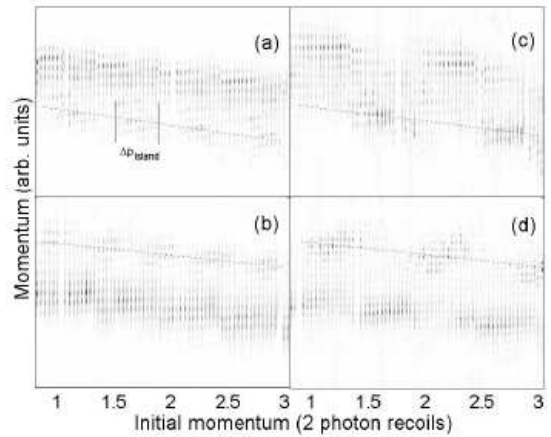


FIG. 3: Experimental momentum distributions showing the sensitivity of the QAMs to the initial conditions. The data is taken after applying 10 kicks with pulse intervals of (a) 61  $\mu\text{s}$  and (b) 72.2  $\mu\text{s}$  and 30 kicks with pulse intervals of (c) 28.5  $\mu\text{s}$  and (d) 37.1  $\mu\text{s}$ . The larger number of kicks at the half-Talbot time was necessary due to the smaller momentum transfer per pulse. The initial momentum was changed by applying the kicking potential with variable time delays after releasing the condensate from the CO<sub>2</sub> laser. The slope of the data seen in this figure is caused by the momentum gain due to gravity. The dotted lines denote the position of the QAM. Note that  $\Delta p_{\text{island}}$  is related to the size of the stability islands by  $\Delta p_{\text{island}} = \hbar G \Delta J_{\text{island}} / \tau$ .

the corresponding experimental values of  $K$ . The experimental and theoretical values for the momentum extent of the islands are given in Fig. 4, near (a) half-Talbot and (b) Talbot times. The circle and asterisk signs are the experimental and theoretical values for  $\Delta J_{\text{island}}$  (as defined in Figs. 2 and 3). It can be seen that the experimental values are very close to the theoretical predictions. Note that for values of  $K > 2$  at half-Talbot time, the stability island elongates in  $J$  and becomes narrow in  $\theta$ . This behavior reduces the effective overlap between the BEC's wavefunction and the stability island and consequently the QAMs were not visible in Fig. 4(b) for higher values of  $K$ . Figure 3 also shows that there can be little overlap between the initial conditions that will populate a QAM at two different values of  $T$ . This behavior particularly affects what happens in experiments in which the momentum distribution is measured as the pulse period is scanned across a resonance time. Unlike the experiments with cold atomic samples where the QAMs on both sides of a resonance could be populated [15], in the case of the condensate, only the QAMs which have significant overlap with the condensate wavefunction will be observable. This can be seen in Fig. 5, where we performed a scan of pulse period across the Talbot time for two different initial momenta. The initial momentum for Fig. 5(a) was set to  $1.2\hbar G$  such that the QAMs were efficiently loaded

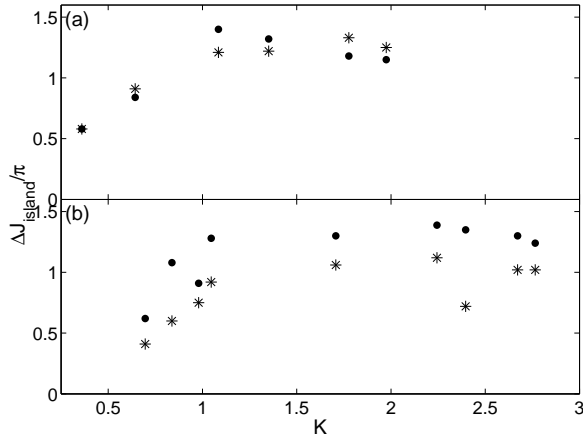


FIG. 4: Experimental data showing the momentum range in which the QAMs appear and the corresponding theoretical predictions. (a) shows the experimental (circle) and theoretical (asterisk) values for  $\Delta J_{\text{island}}$  near half-Talbot time and (b) show the same quantities near Talbot time. Figure 3 illustrates the method used to experimentally infer  $\Delta J_{\text{island}}$ .

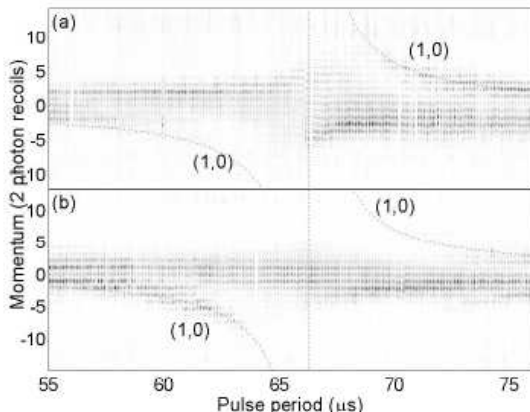


FIG. 5: Experimental momentum distributions showing controllable loading of the  $(p, m) = (1,0)$  QAM. The data was taken by applying 10 kicks for a range of kicking pulse periods. In (a) the initial momentum was set to  $1.2\hbar G$  so as to efficiently create the QAM at pulse periods greater than the Talbot time while in (b) it was set to  $1.5\hbar G$  to efficiently create the QAM at pulse periods smaller than the Talbot time. The curves show the position of the QAM calculated with Eq. (3).

at pulse periods near  $T = 72\mu\text{s}$ , whereas in Fig. 5(b), the initial momentum was set at  $1.5\hbar G$  to mainly populate the QAMs around pulse periods near  $T = 61\mu\text{s}$ . As can be seen, the QAM with indices  $(p, m) = (1,0)$  appear at pulse periods greater than the Talbot time in Fig. 5(a), whereas in Fig. 5(b) the  $(1,0)$  QAM mostly appears at pulse periods smaller than the Talbot time. Note that this is the first time that it has been possible to selectively populate an island at a particular position in phase

space.

In conclusion our experiments have demonstrated the feasibility of observing quantum accelerator modes using a BEC. Using a BEC we were able to examine the underlying pseudo-classical phase space structure of the quantum delta kicked accelerator. These experiments pave the way towards further investigation of more complex systems like the kicked harmonic oscillator [23, 24] and dynamical tunneling [25, 26] that have received little study. This experiment also opens the door to experimental observation of many phenomena related to quantum chaos. For example, the high momentum resolution of the experiment could bring the possibility of observing bifurcation of the stability islands to a practical level. This should lead to a better understanding of the transition to chaos in a quantum system.

---

- [1] A.J. Lichtenberg and M.A. Lieberman, "Regular and chaotic Dynamics" Springer-Verlag, New York (1992).
- [2] F.L. Moore *et al.*, Phys. Rev. Lett. **75**, 4598 (1995).
- [3] C. Ryu *et al.*, Phys. Rev. Lett. **96**, 160403 (2006).
- [4] F.L. Moore *et al.*, Phys. Rev. Lett. **73**, 2974 (1994).
- [5] J. Ringot, P. Sriftgiser, J.C. Garreau, and D. Delande Phys. Rev. Lett. **85**, 2741 (2000).
- [6] H. Ammann, R. Gray, I. Shvarchuck, and N. Christensen, Phys. Rev. Lett. **80**, 4111 (1998).
- [7] G.J. Duffy *et al.*, Phys. Rev. E **70**, 056206 (2004).
- [8] W.H. Oskay, D.A. Steck, V. Milner, B.G. Klappuf, M.G. Raizen, Opt. Comm. **179**, 137 (2000).
- [9] M. Sadgrove, S. Wimberger, S. Parkins, and R. Leonhardt, Phys. Rev. Lett. **94**, 174103 (2005).
- [10] S. Fishman, I. Guarneri, and L. Rebuzzini, J. Stat. Phys. **110**, 911 (2003); *ibid*, Phys. Rev. Lett. **89**, 084101 (2002).
- [11] C.F. Bharucha *et al.*, Phys. Rev. E **60**, 3881 (1999).
- [12] M.B. d'Arcy *et al.*, Phys. Rev. Lett. **87**, 074102 (2001).
- [13] M.V. Berry and E. Bodenschatz J. Mod. Opt. **46**, 349 (1999).
- [14] R.M. Godun *et al.*, Phys. Rev. A **62**, 013411 (2000).
- [15] M.K. Oberthaler *et al.*, Phys. Rev. Lett. **83**, 4447 (1999).
- [16] A. Buchleitner *et al.*, Phys. Rev. Lett. **96**, 164101 (2006).
- [17] M.B. d'Arcy, R.M. Godun, D. Cassettari, and G.S. Summy, Phys. Rev. A **67**, 023605 (2003).
- [18] S. Schlunk, M.B. d'Arcy, S.A. Gardiner, and G.S. Summy, Phys. Rev. Lett. **90**, 124102 (2003).
- [19] L. Deng *et al.*, Phys. Rev. Lett. **83**, 5407 (1999).
- [20] P. Ahmadi, G. Behin-Aein, B.P. Timmons, and G.S. Summy, J. Phys. B **39**, 1159 (2006).
- [21] P. Ahmadi, B.P. Timmons, and G.S. Summy, Phys. Rev. A **72**, 023411 (2005).
- [22] T. Kinoshita, T. Wenger, and D.S. Weiss, Phys. Rev. A **71**, 011602(R) (2005).
- [23] S.A. Gardiner, D. Jaksch, R. Dum, J.I. Cirac, and P. Zoller, Phys. Rev. A **62**, 023612 (2000).
- [24] G.J. Duffy, A.S. Mellish, K.J. Challis, and A.C. Wilson, Phys. Rev. A **70**, 041602(R) (2004).
- [25] D.A. Steck, W.H. Oskay, and M.G. Raizen, Science **293**, 274 (2001).
- [26] W.K. Hensinger *et al.*, Nature **412**, 52 (2001).